AIAA JOURNAL
Vol. 35, No. 7, July 1997

Nonequilibrium Effects in Near-Wake Ionizing Flows

F. Grasso* and S. Pirozzoli†
University of Rome "La Sapienza," Rome 00184, Italy

An analysis of thermal and chemical nonequilibrium effects in near-wake ionizing flows is presented. The influence of real-gas effects on the establishment of scaling laws of the near-wake properties is analyzed, and a simplified model, which relies on an idealized flow solver still capable of accounting for dissociation and ionization effects, is developed. A study of the flows around sphere–cone and Apollo-like re-entry capsule bodies shows that the forebody nonequilibrium does affect the quantities that characterize the near-wake behavior (e.g., upstream influence, extent of recirculation, peak heating along the base). In addition, we show that real-gas effects can be recovered by means of an idealized-gas model that solves for the compressible Navier–Stokes equations and a transport equation for the specific-heat ratio γ, supplemented with algebraic relations to determine the species mass fractions and vibrational temperature as a function of γ.

Nomenclature

D = diffusion coefficient
E = total energy
e = internal energy, electron charge
n = outward unit normal
$\boldsymbol{R}$ = vector of residuals
R_n = nose radius
r = radial coordinate
S = thermal nonequilibrium source term
V = cell volume
$\boldsymbol{W}$ = vector of unknown
X = molar fraction
Y = mass fraction
γ = specific heat ratio
Δh° = enthalpy of formation
Δs = cell face length
η = thermal conductivity
θ = characteristic temperature
μ = mixture viscosity
τ = relaxation time
$\dot{\omega}$ = chemical nonequilibrium source term

Subscripts

ax = wake centerline
b = base
d = dissociation
ds = dividing streamline
E = inviscid contribution, electronic
e = electronic, electron
el = free electron
mol = molecular species
R = removal
rot = rotational
s, r = sth, rth species
sh = edge of boundary layer at the shoulder
T = translational
tr = translational, translation–rotation
V = viscous contribution, vibrational-electron-electronic
v = vibrational

Superscripts

e = electronic
s = sth species
T = transpose
$+$ = ion

Introduction

THE objective of the present work is to assess the influence of thermochemical nonequilibrium on near-wake flows, whose characterization and understanding are crucial for the design of re-entry vehicles.

Figure 1 shows a sketch of a typical flowfield. The forebody region is dominated by a strong bow shock b, which causes a deceleration of the flow; as a consequence, high values of pressure, temperature, and density are reached. At the shoulder, the flow expands and freezes rapidly e, and the boundary layer detaches, forming a free shear layer s that separates the inner recirculation region behind the base from the outer flowfield. The latter is recompressed and turned back to the freestream direction by the so-called lip-shock ℓ and then by a strong recompression shock r. At the end of the recirculation zone, past the neck n, the shear layer develops in the wake trail t, which is often turbulent and unsteady. Nonequilibrium effects are mainly confined in the forebody region, whereas the near base recirculating region is generally expected to be frozen.[1–4] The freezing of the flow (hence, the thermodynamic properties and composition in the near wake) depends on the geometry and flow conditions, and strongly affects critical design quantities, for example, peak heating that depends on the mixture composition. In addition, as a consequence of the strong recompression around the neck, nonequilibrium effects may again occur in this region.

Gnoffo et al.[1] reported simulations of the near-wake flowfield behind aerobrakes, assuming thermal and chemical nonequilibrium throughout, and showed the influence of nonequilibrium phenomena on the shear-layer deflection (and its interaction with the payload) and the consequent increase in peak heating in the base region. In addition, a reduction of the Reynolds number has been shown to produce a delay in the shear layer separation.[1,2] The effects of rarefaction, surface temperature, and corner shape on the near wake of a 70-deg blunt cone have been shown by means of a direct simulation Monte Carlo method.[5] The base region is found to be affected by thermal nonequilibrium; in addition, a stable vortex (whose size is shown to increase with the freestream Knudsen number) is obtained only at low Knudsen numbers and no lip shock or recirculation shock arise when rarefaction effects are significant. Dogra et al.[5] also show that high local Knudsen numbers are reached just after the shoulder, even at low altitudes, thus raising some doubts about the applicability of continuum models. Kim et al.[6] have investigated the effects of gas models on hypersonic base flows, showing in particular the influence of thermochemical nonequilibrium on the near-wake extent and the rear stagnation-point location.

Received Aug. 5, 1996; revision received Feb. 26, 1997; accepted for publication April 8, 1997.

*Associate Professor, Department of Mechanics and Aeronautics, Via Eudossiana, 18. Associate Fellow AIAA.
†Graduate Student, Department of Mechanics and Aeronautics, Via Eudossiana, 18.

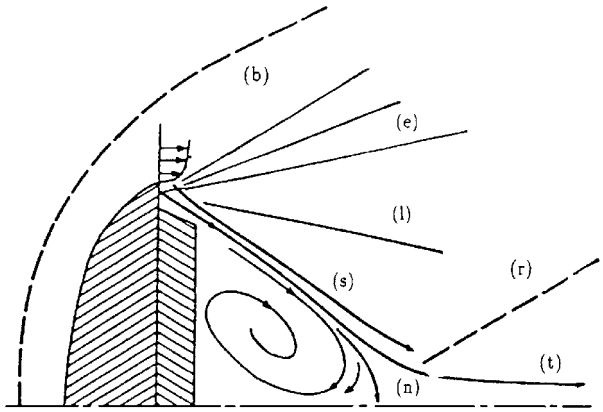

Fig. 1 Near-wake flow: *b*, bow shock; *e*, expansion; *s*, free shear layer; *l*, lip shock; *r*, recompression shock; *n*, wake neck; and *t*, wake trail.

Mitcheltree and Gnoffo[7] have analyzed the near-wake flow about a Mars entry vehicle that enters into Mars atmosphere at 7.65 km/s, and have concluded that the near-wake flow does not exhibit significant nonequilibrium effects. Venkatapathy et al.[4] assumed fully frozen conditions in the base region and devised a strategy that solves for the conservation equations for thermochemical nonequilibrium in the forebody region, and the ideal Navier–Stokes equations in the afterbody region. Computations of flows around the body used in the Aeroassisted Flight Experiment show that the ideal-gas results qualitatively agree with those obtained with full real-gas simulations. Grasso and Pettinelli[2] have contributed to the characterization of the near wake by assuming an ideal-gas behavior, and have found that the flow in the near wake satisfies scaling laws. In particular, they show that the location of the upstream influence of the base, i.e., the upstream effect of the flow expansion around the shoulder, and the separation depend on the forebody boundary-layer properties, as well as on the shear layer that develops at the shoulder. The same holds true for the extent and shape of the near-base recirculation zone, and for the fluid-dynamic character of the near wake, i.e., convection–diffusion-dominated behavior.

The scope of the present work is twofold: 1) we analyze the influence of real gas effects on the establishment of scaling laws for the near-wake properties; and 2) we develop a simplified model that relies on an idealized flow solver still capable of accounting for dissociation and ionization effects. In particular, we show that the near-wake flow can be properly characterized by means of a model based on the solution of the Navier–Stokes equations coupled with a transport equation for a mixture thermodynamic property (for example, the specific heat ratio γ), provided that an algebraic dependency of the mixture composition and vibrational temperature upon γ is determined.

In the following, we first describe the complete flow model for weakly ionizing flows in thermochemical nonequilibrium and then develop the simplified idealized model. Results of simulations around sphere–cone and Apollo-like bodies are discussed, and some concluding remarks are given.

Governing Equations

Nonequilibrium Gas Model

We first describe the governing equations for a mixture of gases in thermal and chemical nonequilibrium. The model assumes that a single translational temperature T characterizes the translational and rotational modes, whereas a single temperature T_V characterizes the vibrational and electronic modes of heavy particles and the translational modes of free electrons (hereafter referred to as vibrational-electron-electronic). Moreover, neglecting externally applied electric and magnetic fields, it is assumed that charge separation and conduction currents are negligible. In vector form, the conservation equations are

$$\frac{\partial}{\partial t}\int_V \boldsymbol{W}\,\mathrm{d}V + \oint_S (\boldsymbol{F}_E - \boldsymbol{F}_V)\cdot\boldsymbol{n}\,\mathrm{d}S = \int_V \boldsymbol{H}\,\mathrm{d}V \qquad (1)$$

where

$$\boldsymbol{W} = [\rho_s,\ \rho u,\ \rho v,\ \rho E,\ \rho e_V]^T$$

$$\boldsymbol{F}_E = [\rho_s \boldsymbol{u},\ \rho \boldsymbol{u}\otimes\boldsymbol{u} + p\boldsymbol{I},\ \rho \boldsymbol{u}H,\ \rho \boldsymbol{u}e_V]^T$$

$$\boldsymbol{F}_V = [-\rho_s \boldsymbol{V}_s,\ \sigma,\ \sigma\cdot\boldsymbol{u} - \boldsymbol{Q},\ -\boldsymbol{Q}_V]^T$$

$$\boldsymbol{H} = [\dot{\omega}_s,\ 0,\ 0,\ 0,\ S_V]^T$$

and

$$\rho_s \boldsymbol{V}_s = -\rho D_s \nabla X_s$$

$$\sigma = \mu(\nabla\boldsymbol{u} + \nabla\boldsymbol{u}^T) - \tfrac{2}{3}\mu(\nabla\cdot\boldsymbol{u})\boldsymbol{I}$$

$$\boldsymbol{Q} = -(\eta_{tr} + \eta_{rot})\nabla T - (\eta_v + \eta_E + \eta_{el})\nabla T_V - \sum \rho h_s D_s \nabla X_s$$

$$\boldsymbol{Q}_V = -(\eta_v + \eta_E + \eta_{el})\nabla T_V - \sum \rho h_V^s D_s \nabla X_s$$

$$E = \sum Y_s e_s + \frac{u^2 + v^2}{2}, \qquad H = E + \frac{p}{\rho}$$

$$\rho = \sum \rho_s, \qquad p = \sum \rho_s R_s T + p_e, \qquad p_e = \rho_e R_e T_V$$

The internal energy of species s is obtained assuming energy mode separability.[8,9] For atomic species, one has

$$e_s = \tfrac{3}{2}R_s T + e_E^s + \Delta h_s^\circ$$

whereas for diatomic species, one obtains

$$e_s = \tfrac{5}{2}R_s T + e_v^s + e_E^s + \Delta h_s^\circ$$

and the vibrational and electronic energy contributions are obtained assuming Boltzmann distributions at the vibrational-electron-electronic temperature T_V, thus yielding

$$e_v^s = R_s \theta_s^v \frac{1}{\exp(\theta_s^v / T_V) - 1}$$

$$e_E^s = R_s \frac{\sum_{j=1,N_s^e} g_{s,i}\theta_{s,i}^e \exp(-\theta_{s,i}^e / T_V)}{\sum_{j=1,N_s^e} g_{s,i}\exp(-\theta_{s,i}^e / T_V)}$$

where the electron translational energy is given by $e_{el} = \frac{3}{2}R_e T_V$ and $g_{s,i}$ is the ith-state degeneracy.[8–10]

The mixture viscosity, the thermal conductivity, and the diffusion coefficients are determined according to Chapman–Enskog theory and an extension of the Yos formula.[11,12] In addition, under a weakly ionized gas assumption, the effective diffusion coefficient of the electrons D_e is proportional to the ambipolar diffusion coefficient of the ions.[13,14]

Finite rate chemistry has been modeled by using an 18-reaction mechanism[10] and a nonpreferential coupling model for both dissociation and ionic recombination reactions.[10,12] The vibrational-electron-electronic source term is

$$S_V = -p_e \nabla\cdot\boldsymbol{u} + S_{T-v} + S_{T-E} + S_{V-R}$$

where the term $-p_e\nabla\cdot\boldsymbol{u}$ is related to the work of the electric field. The translation–vibration energy exchanges are modeled according to Landau–Teller theory[8–10]:

$$S_{T-v} = \sum \rho_s \frac{e_v^s(T) - e_v^s(T_V)}{\tau_s}$$

where the vibrational relaxation time is defined as the sum of the molar-averaged Millikan–White[15] relaxation time τ_s^{M-W} and the collision-limited time τ_s^P, as described elsewhere.[12] Neglecting frictional heating of the electrons (due to differences between the electron and heavy-particle velocities), the heavy-particle electron-electronic energy exchanges are

$$S_{T-E} = 2m_e n_e \sum \frac{3}{2}\frac{k}{m_r}(T - T_V)\,\nu_{er}^*$$

where k is the Boltzmann constant and ν_{er}^* is the collision frequency that is determined as suggested elsewhere.[12,16,17] The energy removal contribution due to coupling between chemistry and vibration and to electron-electronic excitations has been assumed to be related to the average vibrational and electron-electronic energies, as also assumed elsewhere,[3,11,16] i.e.,

$$S_{V-R} = \dot{\omega}_e e_{el} + \sum \dot{\omega}_s e_V^s$$

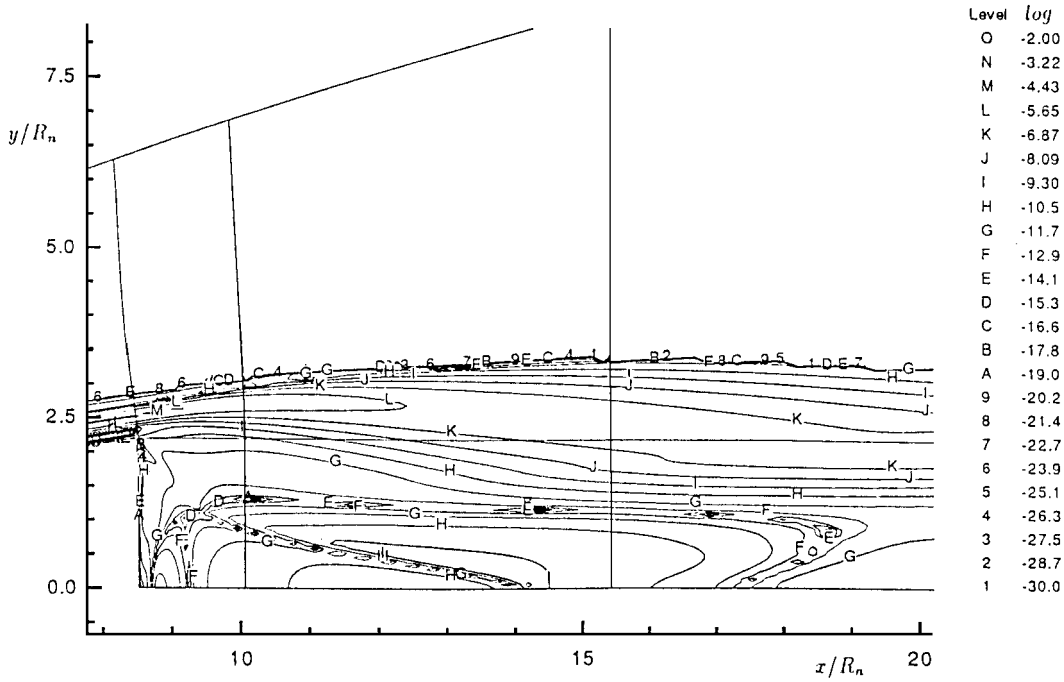

a) Chemical Damköhler (Da_c)

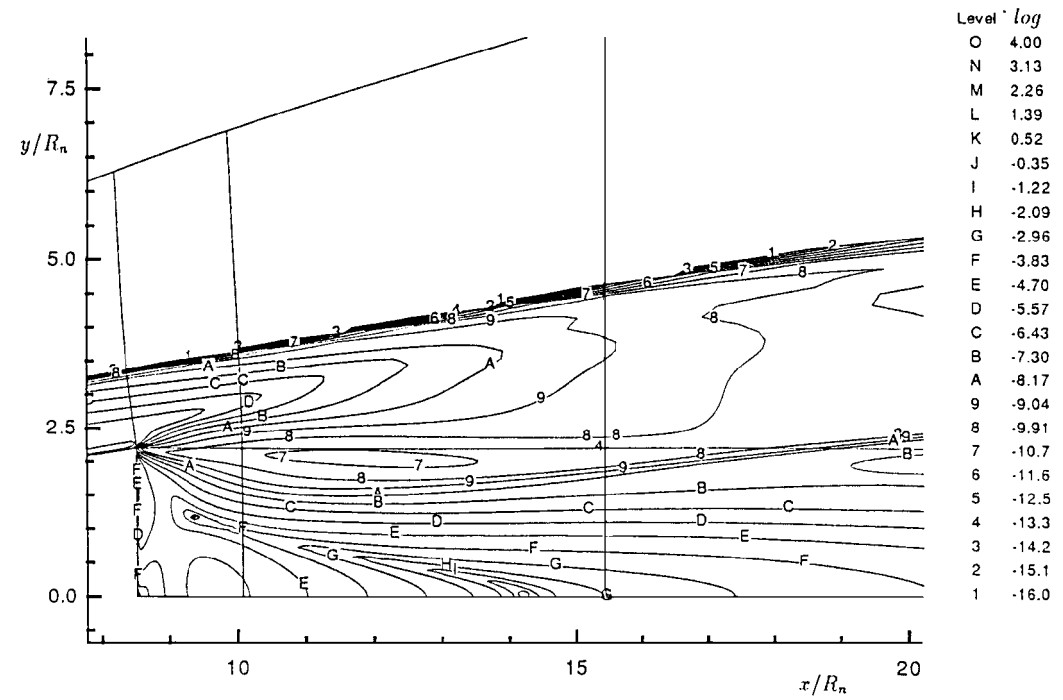

b) Vibrational Damköhler (Da_v)

Fig. 2 Iso-Damköhler contour lines (in log scale).

Idealized-Gas Model

It has been pointed out that the formation of the near wake is mainly a fluid-dynamic phenomenon controlled by the flow expansion that occurs around the corner, and that is responsible for the freezing of the flow in the base region.[2] The intensity of the expansion depends on the upstream flow properties, i.e., the forebody nonequilibrium effects (primarily through the specific-heat ratio). We point out that a frozen-flow assumption is certainly valid in the outer region of the near wake; however, the very-near base flow region is controlled by two competing mechanisms: 1) the expansion of the flow, which yields an increase in the relaxation time scales; and 2) the trapping of the gas mixture in the recirculation zone, which produces an increase in the residence time scale. Let Da_v and Da_c be, respectively, the local thermal and chemical Damköhler numbers, given by

$$Da_v = b/v\,\tau_v, \qquad Da_c = b/v\,\tau_c$$

where we have defined the vibrational and chemical time scales according to

$$\frac{1}{\tau_v} = \sum_s \frac{\beta_s}{\tau_{v,s}}, \qquad \frac{1}{\tau_c} = \sum_s Y_s \frac{\dot{\omega}_s}{\rho}$$

and β_s accounts for the contribution onto the mixture vibrational energy of the heavy (molecular) species

$$\beta_s = \frac{Y_s e_{v,s}}{\sum_r Y_r e_{v,r}}$$

In Fig. 2, we report the iso-Da_v and the iso-Da_c for the nonequilibrium flow around a sphere–cone geometry corresponding to test case A of Table 1. Figure 2 shows that the flow in the near wake can indeed be assumed to be frozen. However, the mixing process, which occurs across the dividing streamline, plays a major role in the establishment of the thermochemical properties of the near wake, as one

Table 1 Test-case conditions

Test	Geometry	Altitude, km	Speed, m/s	Re_∞	M_∞
A	RAM-C	61	7,650	4.72835×10^4	23.96
B	RAM-C	71	7,650	1.34884×10^4	25.87
C	RAM-C	61	5,100	3.15227×10^4	15.98
D	RAM-C	61	11,500	7.0952×10^4	38.80
E	ARC	61	5,486	1.740321×10^5	17.51
F	ARC	71	8,230	7.60315×10^4	27.88

can infer from Fig. 3, where we report the budgets of the vibrational energy and the atomic oxygen vs the distance from the wake axis in the core of the recirculation region. Figure 3 indeed shows that mass and energy transfers occur along the dividing streamline, primarily through a balance between convection and diffusion effects.

Thermally and chemically frozen conditions can be assumed in the outer region, roughly at a distance from the nose of $O(R_n)$ for the sphere–cone geometry here investigated, and near the shoulder for the re-entry capsule. However, in general, the assumption may raise some doubts about its validity in the recirculation region. Indeed,

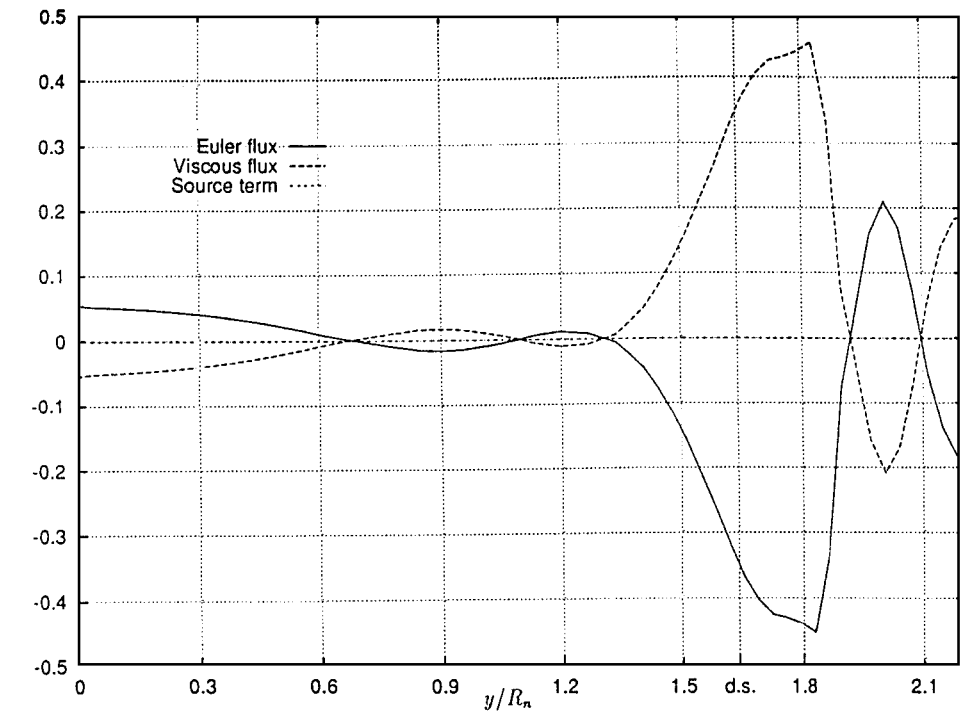

a) Vibrational energy

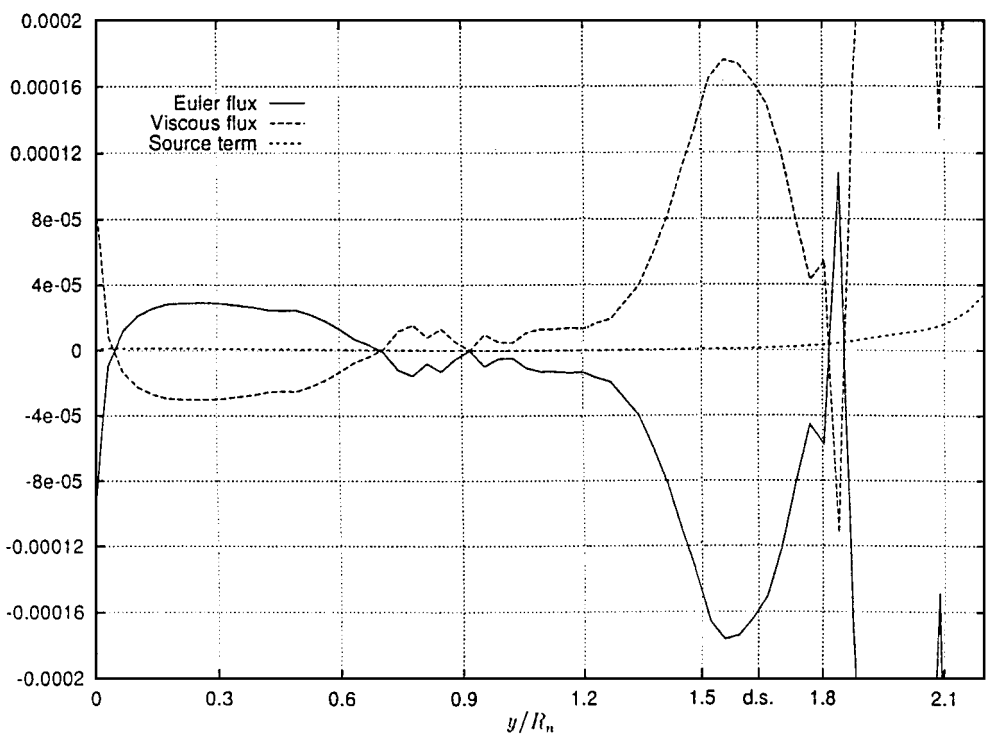

b) Atomic oxygen

Fig. 3 Budgets within the recirculation core.

downstream of the neck, because of the strong recompression, the local temperature increase may activate finite rate energy transfers, and the frozen-condition assumption may fail.

The development of the idealized-gas model relies on the compressible Navier–Stokes equations; however, to account for the influence of the forebody real-gas effects (on the gas constant and on the specific-heat ratio), we include a transport equation for γ, which is defined as

$$\gamma = h_{\mathrm{tr}}/c_{\mathrm{tr}} = 1 + R/c_{v,\mathrm{tr}}$$

where R is the gas constant

$$R = \sum_s R_s Y_s$$

and $c_{v,\mathrm{tr}}$ is the translation–rotation constant-volume specific-heat coefficient of the mixture

$$c_{v,\mathrm{tr}} = \sum_s \alpha_s R_s Y_s$$

with $\alpha_s = \frac{3}{2}$ for atomic and $\alpha_s = \frac{5}{2}$ for diatomic species. From the definition of γ and the frozen-flow assumptions, it is a simple matter to show that γ satisfies a transport equation whose differential form is

$$\frac{\partial \rho\gamma}{\partial t} + \mathrm{div}(\rho \boldsymbol{u}\gamma) = \frac{1}{c_{v,\mathrm{tr}}} \sum_s^N [R_s \phi_s \,\mathrm{div}(\rho D_s \nabla Y_s)] \qquad (2)$$

where $\phi_s = 1 - \alpha_s(\gamma - 1)$.

We observe that 1) Eq. (2) strictly holds in the region where the flow is indeed frozen and 2) even in this region the closure of the equation requires the determination of both Y_s and T_V. As has been pointed out, the nonequilibrium effects are mainly confined in the forebody region (essentially the nose region for the sphere–cone, and extending from the nose to the shoulder location for the re-entry capsule geometry). If one recalls the definition of γ and exploits the analogy between the transport equations of γ and Y_s, one can reason that along each streamline a one-to-one relation $Y_s = Y_s(\gamma)$ exists if one assumes 1) a sudden transition from nonequilibrium to frozen conditions at a location X_{RI} and 2) negligible diffusion effects. Numerical simulations for the conditions of Table 1 show that such a relation holds. In Fig. 4, we report the values of Y_s vs γ obtained from a full real-gas computation, evaluated at three different sections: one located just before the corner, one at the core of the recirculation region, and one farther downstream. The curves reported for atomic and molecular nitrogen clearly show that a relation holds through the entire near-wake flowfield.

Under these assumptions, the idealized-gas model reduces to an ideal-gas model with γ constant along each streamline. However, such a model would fail for two reasons: 1) the value of γ (and Y_s and T_V) in the recirculation region would be arbitrary; and 2) the diffusion effects are not truly negligible (as shown in Fig. 3). Therefore, to remove such arbitrariness, the diffusion effects have not been neglected, but we have assumed that the relation $Y_s = Y_s(\gamma)$ [and $T_V = T_V(\gamma)$] determined at X_{RI} holds at any other location. We remark that the model is not strictly justifiable on theoretical grounds; however, it leads to correct results when compared with the full nonequilibrium ones, as we show in the Results and Discussion section.

Numerical Solution

The solution of the governing equations for high-speed flows requires the use of robust and accurate schemes. We have used a finite volume formulation that relies on a second-order upwind-biased total variation diminishing (TVD) discretization of the inviscid fluxes and central differencing of the viscous ones. The details of the scheme for the full nonequilibrium simulations[12] and for the idealized-gas model[18] have already been reported; the discretized equations are cast in the following form:

$$V\frac{\mathrm{d}\boldsymbol{W}}{\mathrm{d}t} + \boldsymbol{R} = 0$$

and the residual $\boldsymbol{R}$ is

$$\boldsymbol{R} = \sum_\alpha (\boldsymbol{F}_E - \boldsymbol{F}_V) \cdot \boldsymbol{n}\Delta s - \boldsymbol{H}V$$

where α indicates the generic cell face and $\boldsymbol{H}$ also accounts for terms that arise from the finite volume discretization of axisymmetric geometries ($\boldsymbol{H} = \boldsymbol{H} + \boldsymbol{H}_{\mathrm{ax}}$), with $\boldsymbol{H}_{\mathrm{ax}}$ being a vector whose nonzero component ($h_{\mathrm{ax},\,v}$) is the one corresponding to the radial momentum equation

$$h_{\mathrm{ax},v} = p - 2\mu\left[(v/r) - \tfrac{1}{3}\nabla \cdot \boldsymbol{u}\right]$$

Time integration is performed by means of an explicit three-stage Runge–Kutta algorithm with local time stepping to accelerate convergence.[12]

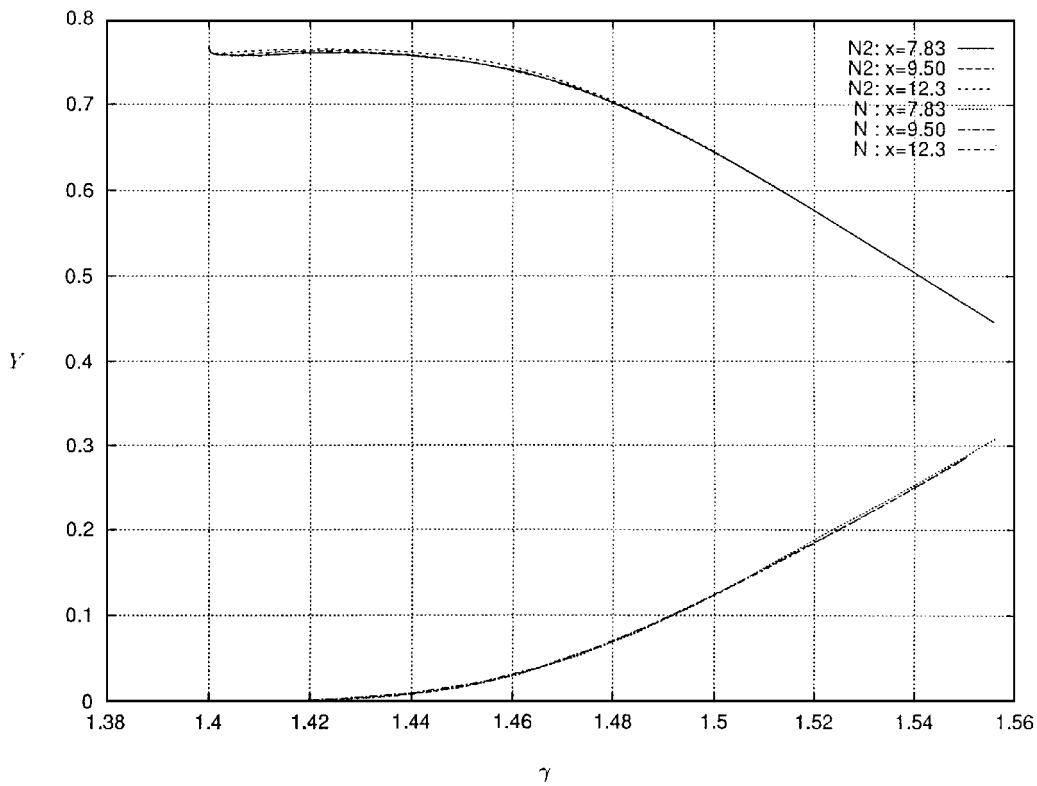

Fig. 4 Atomic and molecular nitrogen mass fraction distributions vs γ for test case A.

With regard to the idealized model formulation, we observe that the transport equation for γ is loosely coupled with the remaining equations. Its finite volume approximation has then been obtained by discretizing the convective flux according to the formulas proposed by Larrouturou[19] for an approximate multicomponent Riemann solver. In particular, the inviscid numerical flux function of γ at a cell interface that separates a left and right state, i.e., the average values of the two adjacent cells, is expressed in terms of the numerical flux function of the total mass, thus yielding

$$(\boldsymbol{F}_{E(\gamma)} \cdot \boldsymbol{n}\Delta s)_{\alpha} = (\boldsymbol{F}_{E(\rho)} \cdot \boldsymbol{n}\Delta s)_{\alpha} \times \begin{cases} \gamma_L & \text{if } \boldsymbol{F}_{E(\rho)} \cdot \boldsymbol{n} \geq 0 \\ \gamma_R & \text{if } \boldsymbol{F}_{E(\rho)} \cdot \boldsymbol{n} < 0 \end{cases}$$

where $\boldsymbol{F}_{E(\ )}$ is the numerical flux of the quantity $(\ )$, obtained as described elsewhere.[18]

Parallel Implementation

Both the real- and idealized-gas solvers employ a subdomain decomposition strategy that exploits parallel architecture by means of an enhanced message-passing paradigm implemented on the IBM SP2 computer available at CASPUR in Rome. The partitioning of the computational domain into subdomains is done in such a way as to balance the load; at the interfaces between adjacent blocks we have imposed the continuity of the variables and conservation of the numerical fluxes. To maintain second-order accuracy, we have introduced two fictitious layers of cells surrounding the blocks, thus enforcing the interface conditions by injecting the solution of the underlying block onto the overlaying one. For an efficient exploitation of the parallelism, we also have treated the block interface communication in a loosely synchronous manner: nodes exchange information only when a synchronization point is reached.

With regard to the speedup, which is defined as the ratio of single processor to n-processors execution times ($S_n = T_1/T_n$), the computed results show a nearly linear speedup (in particular, we obtain $S_8 = 7.08$, $S_{16} = 12.68$), with an efficiency of $O(80\%)$. Note that a typical full real-gas computation on a capsule shape requires approximately 20 h of CPU time with 16 processors, whereas an analogous calculation carried out using the idealized-gas solver requires about 2 h.

Results and Discussion

The objective of the present work is twofold: 1) to assess the influence of nonequilibrium effects on the near-wake flows and 2) to establish the validity of the idealized-gas model. Several computations have been performed for the flows around a sphere–cone geometry (corresponding to the Radio Attenuation Measurement experiment, RAM-C) and a re-entry capsule [hereafter referred to as ARC (Apollo-like re-entry capsule)].

The geometry of the RAM-C is a sphere of 15-cm nose radius with a 9-deg cone, whose length is 130 cm. For all computations, we have used a grid having 218×64 cells in the outer region and 128×64 in the wake region, with mesh spacing ranging from 4.25×10^{-5} m to 5.75×10^{-2} m in the forebody region and from 7.90×10^{-3} m to 4.58×10^{-2} m in the afterbody zone. The geometry of the ARC consists of the command module of the Apollo for the forebody (of length 2.99 m) followed by a cylindrical afterbody (of length 0.489 m). For the ARC geometry, we have used a grid of 208×60 cells in the outer region (with minimum spacing from 4.77×10^{-4} m and minimum spacing of 9.92×10^{-3} m), and 125×30 cells in the wake (with spacing ranging from 9.92×10^{-3} m to 1.72×10^{-1} m).

For the RAM-C geometry the selected grid is sufficient to ensure grid independency,[12] where a grid sensitivity analysis for the same type of problem was discussed. Then a limited grid sensitivity study was carried out only for the ARC geometry. In particular, we have considered the following meshes: grid A1 having a total of $(416 \times 60) + (250 \times 30)$ cells and grid A2 having $(208 \times 120) + (125 \times 60)$ cells, obtained by halving the mesh spacing of the base grid. The computed results (not reported because of space limitations) indicate that the grid resolution in the direction normal to the wall mainly affects the forebody solution, whereas the afterbody solution depends both on the forebody and afterbody mesh resolutions.

Full Nonequilibrium Simulations

To evaluate the influence of thermochemical nonequilibrium effects, we have carried out a parametric study of the flow around the RAM-C and the ARC geometries at different altitudes (61, 71 km); for the RAM-C body, we also have performed computations at different re-entry velocities. The details of the test cases are given in Table 1. The computed and measured[20] peak electron-number densities for the 61- and 71-km RAM-C test cases are reported in Fig. 5,

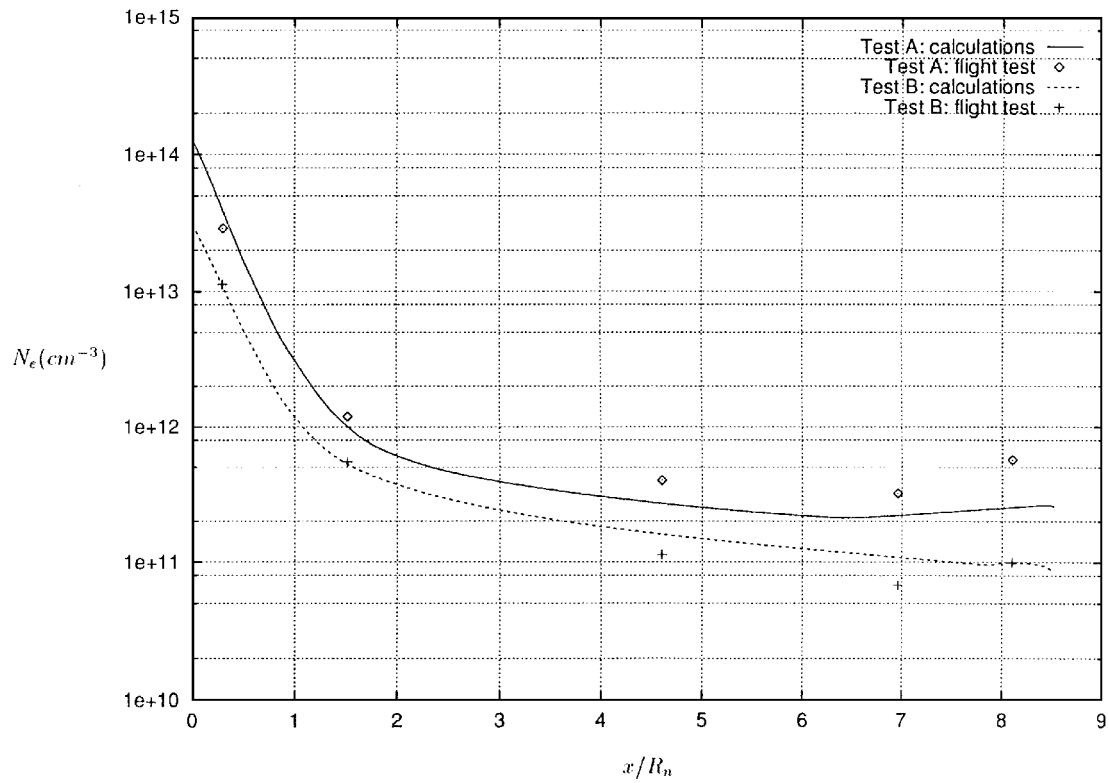

Fig. 5 RAM-C: ——, 61 km computed; - - - -, 71 km computed; ◇ 61 km measured; and + + + +, 71 km measured.

which shows good agreement between computed and experimental results. In addition, Fig. 5 indicates that the influence of the afterbody (by an upstream wave propagation mechanism) on the radio attenuation phenomenon is negligible.

The cold hypersonic laminar near-wake behavior has been analyzed.[2] The latter shows that near-shoulder quantities, such as the Mach (M_{sh}) and Reynolds numbers (Re_{sh}), the wall vorticity, and the thickness of the subsonic portion of the forebody boundary layer (δ_s), as well as near-wake properties [mainly the maximum Reynolds number along the dividing streamline (Re_{ds})], play a fundamental role in the characterization of the near-wake behavior. In particular, Grasso and Pettinelli[2] show that the upstream influence $\Delta\ell$, the location of separation Δs, the wake neck thickness δ_w, and the extent of the primary recirculation ℓ_w, whose ratio identifies the aspect ratio of the near wake and the compressibility effects (measured in terms of the Mach number in the wake) satisfy scaling laws that depend mainly on Re_{ds}. Grasso and Pettinelli[2] apply the boundary-layer concepts in the proximity of the wall at the shoulder and show that one can relate the pressure drop [which occurs over a distance of $\mathcal{O}(\Delta\ell)$] to the skin friction and to δ_s (evaluated at the section immediately before the extent of upstream influence), thus finding a functional dependence of $\Delta\ell$ on the expansion around the corner and Re_{ds}.

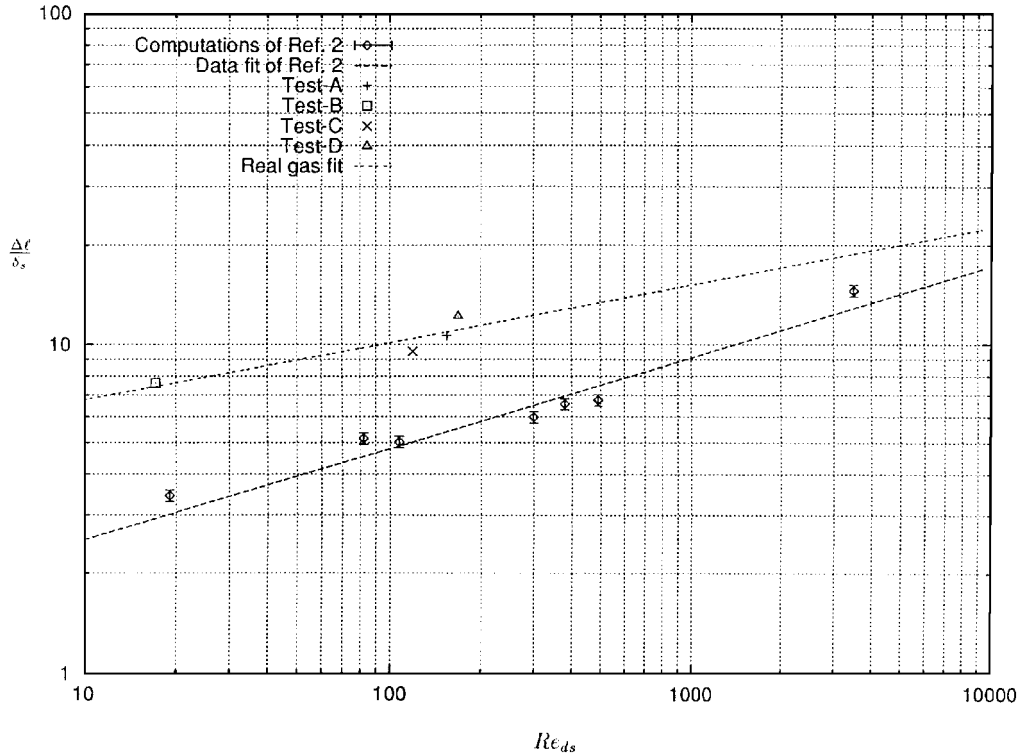

Fig. 6 Upstream influence vs dividing streamline Reynolds number Re_{ds}.

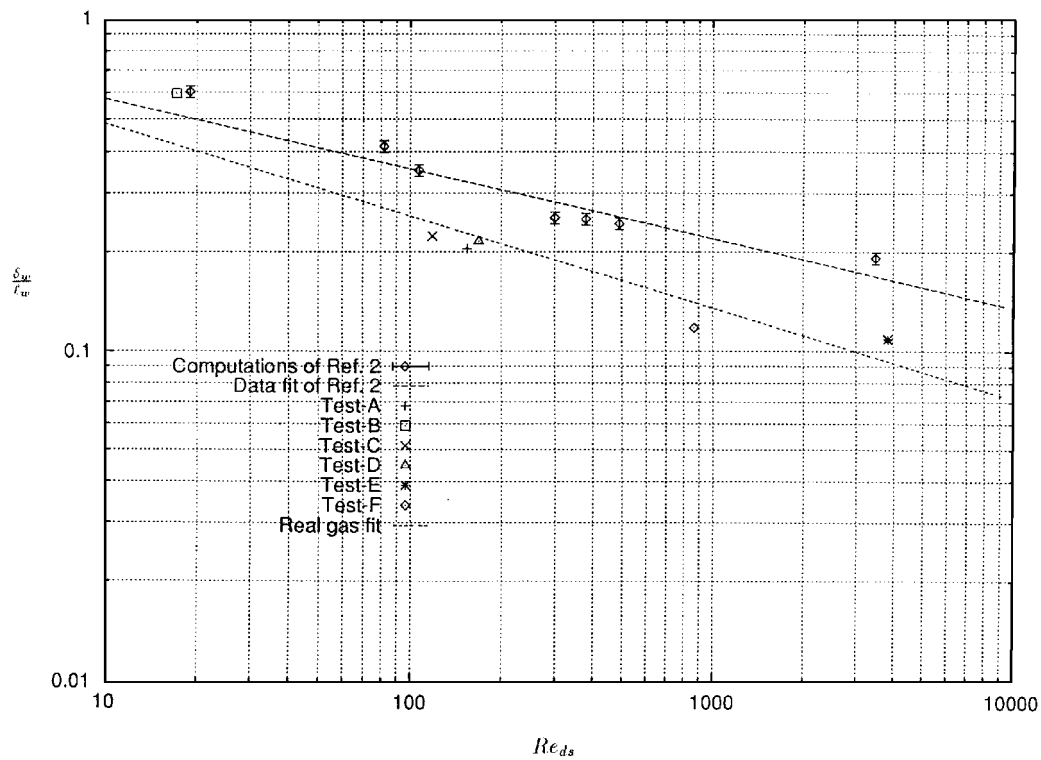

Fig. 7 Wake neck thickness vs Re_{ds}.

The separation on the base is strictly related to the occurrence of a local peak in the pressure gradient along the base, is affected by the upstream propagation of pressure signals through the subsonic portion of the boundary layer and by the Reynolds number,[2,21] and shows a functional dependency on Re_{ds}, δ_s, and the strength of the interaction mechanism (mainly M_{sh}).[2]

With regard to the wake neck thickness and the recirculation extent, for a given (cylindrical) geometry and (hypersonic) Mach number, δ_w is shown to correlate with the boundary-layer thickness at the shoulder and Re_{ds}; at low Re, ℓ_w increases with the Reynolds number, whereas at high Re it approaches a value that is rather independent of the Reynolds number.[2] In addition, Grasso and Pettinelli[2] show that the effects of compressibility in the near-wake region can be characterized in terms of the maximum Mach number along the dividing streamline (M_{ds}) and the maximum one on the symmetry axis (M_{ax}), which show a scaling-law dependency on Re_{ds}.

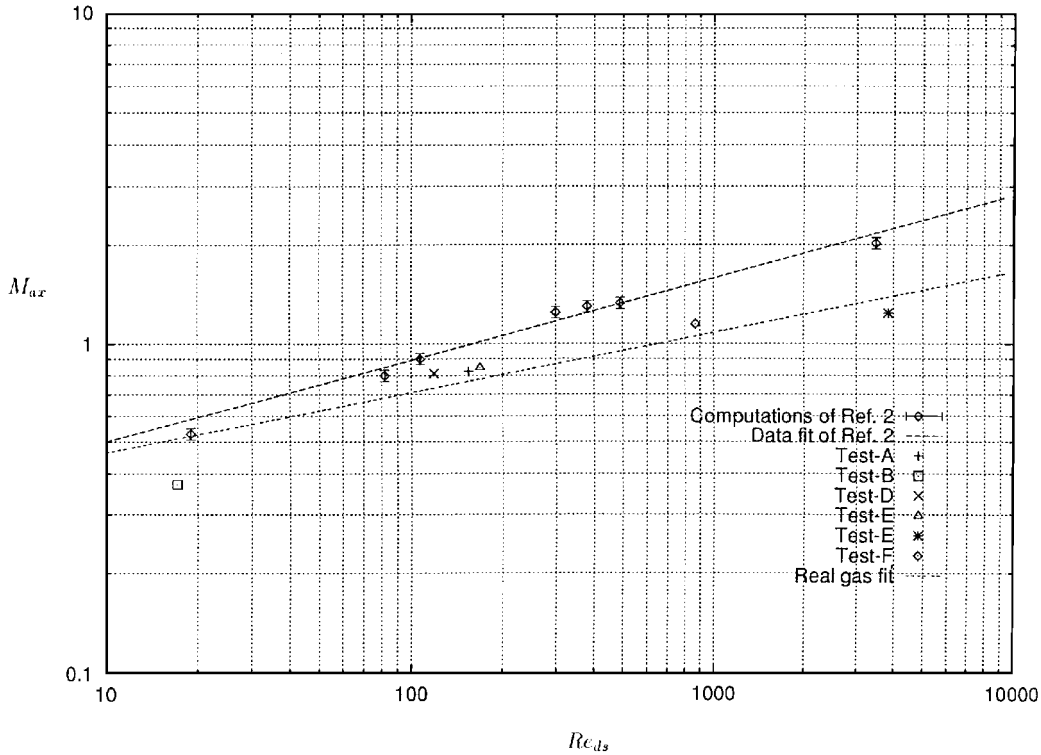

Fig. 8 Centerline maximum Mach number vs Re_{ds}.

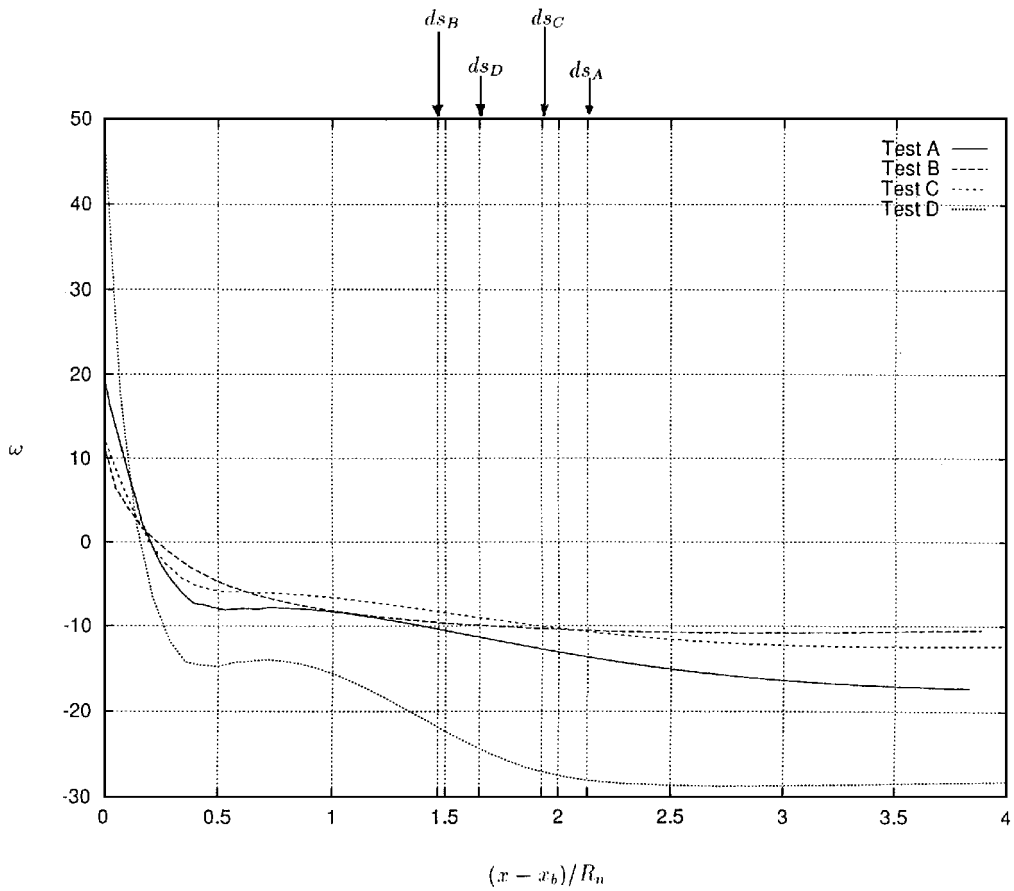

Fig. 9 Streamwise vorticity distribution in recirculation core (RAM-C test case A); ds, intersection with dividing streamline.

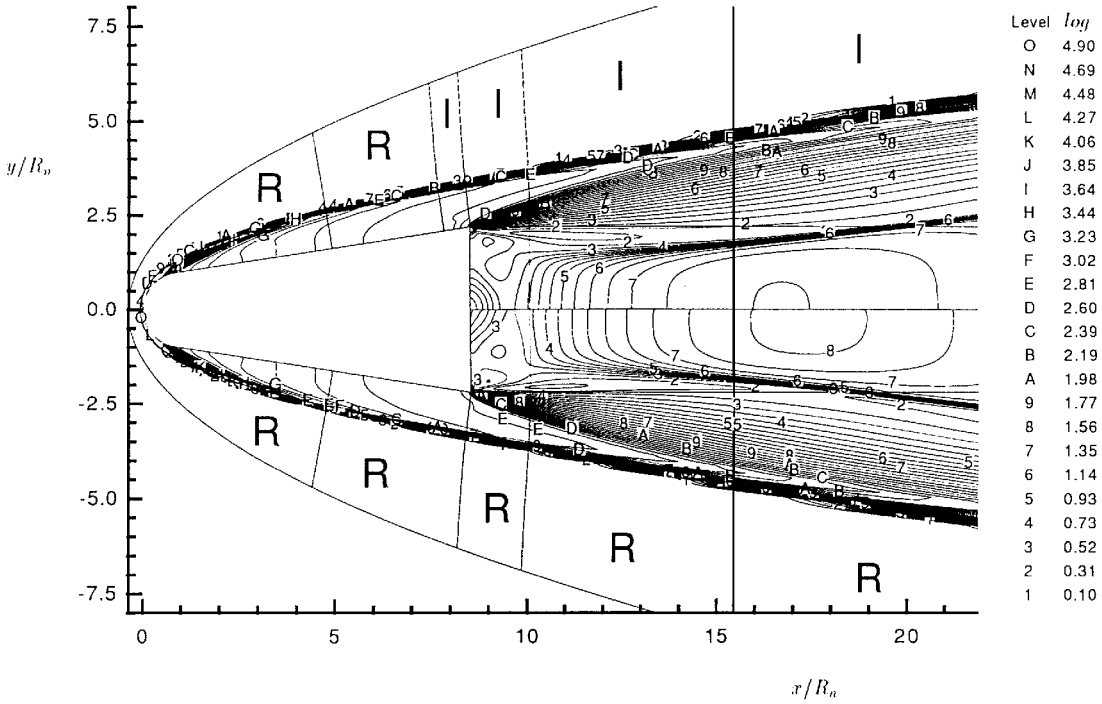

Fig. 10 Isopressure contour lines (in log scale) for test case A: *I*, idealized-gas solution and *R*, full real-gas solution.

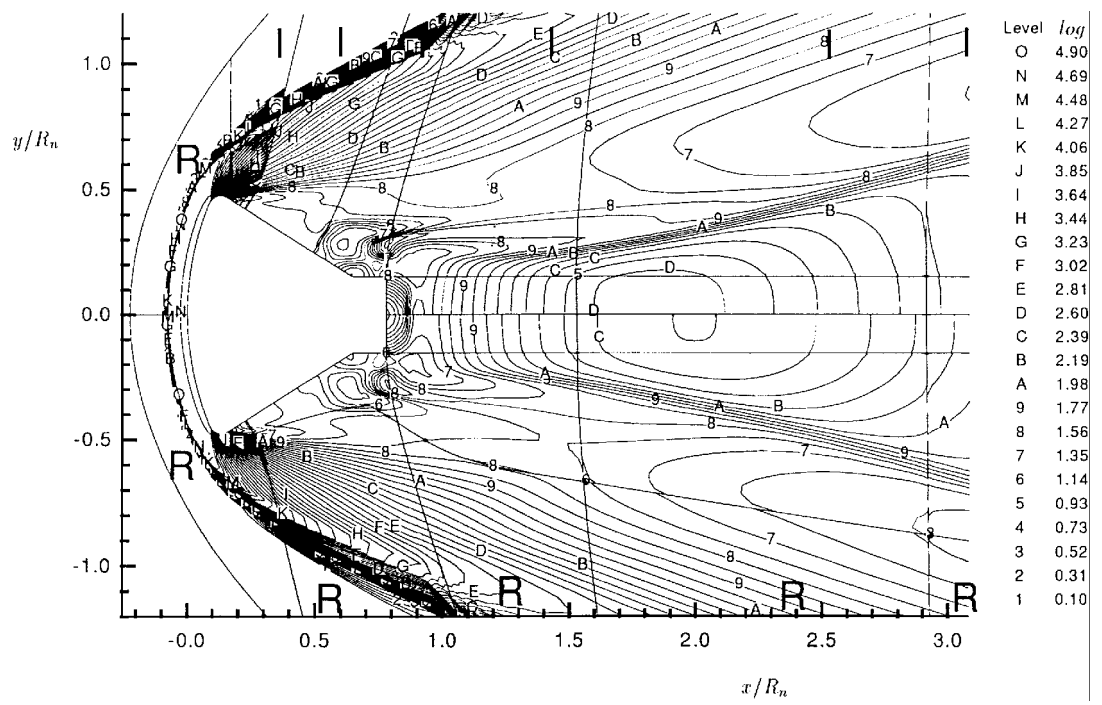

Fig. 11 Isopressure contour lines (in log scale) for test case E: *I*, idealized-gas solution and *R*, full real-gas solution.

Note that, even in the presence of nonequilibrium effects, the near-wake properties satisfy scaling laws that depend mainly on Re_{ds} as found for cold hypersonic conditions, as Figs. 6–8 indicate. However, the results show an increase (with respect to cold hypersonic simulations) in the extent of the recirculating region (a consequence of the weaker expansion around the shoulder), and an increase in the aspect ratio of the near wake, i.e., the near wake is more elongated. Another interesting observation is on the upstream influence extent, which increases if one accounts for real-gas effects. A possible explanation for this is in the reduction of the difference between the peak temperature in the boundary layer and the wall temperature, i.e., the wall behaves as if it were "less cold," and in the increase of δ_s. As a consequence, the increase in the upstream influence is to be expected. From the computations, we then find

$$\Delta\ell/\delta_s \propto Re_{ds}^{0.18}, \qquad \Delta s/\delta_s \propto Re_{ds}^{-0.6} M_{sh}^{0.9}, \qquad \delta_w/\ell_w \propto Re_{ds}^{-0.3}$$

$$M_{ds} \propto Re_{ds}^{0.2}, \qquad M_{ax} \propto Re_{ds}^{0.18}$$

where the dividing streamline Reynolds number satisfies $Re_{ds} \propto Re_{sh}^{1.6} M_{sh}^{-3.8}$. As already observed in the study of cold near-wake flows,[2] a relationship between the behavior of the recirculation region and Re_{ds} exists: The wake is either convection- or diffusion-like, depending on the value Re_{ds}. From the simulations, we find that Re_{ds} also affects the structure of nonequilibrium near-wake flows. The vorticity distribution within the recirculation (reported in Fig. 9) shows that for the RAM-C cases, $Re_{ds} \simeq \mathcal{O}(10^2)$ and no constant vorticity core arise, i.e., a diffusion-like near wake is established. On the other hand, for the ARC shape (whose results are not reported

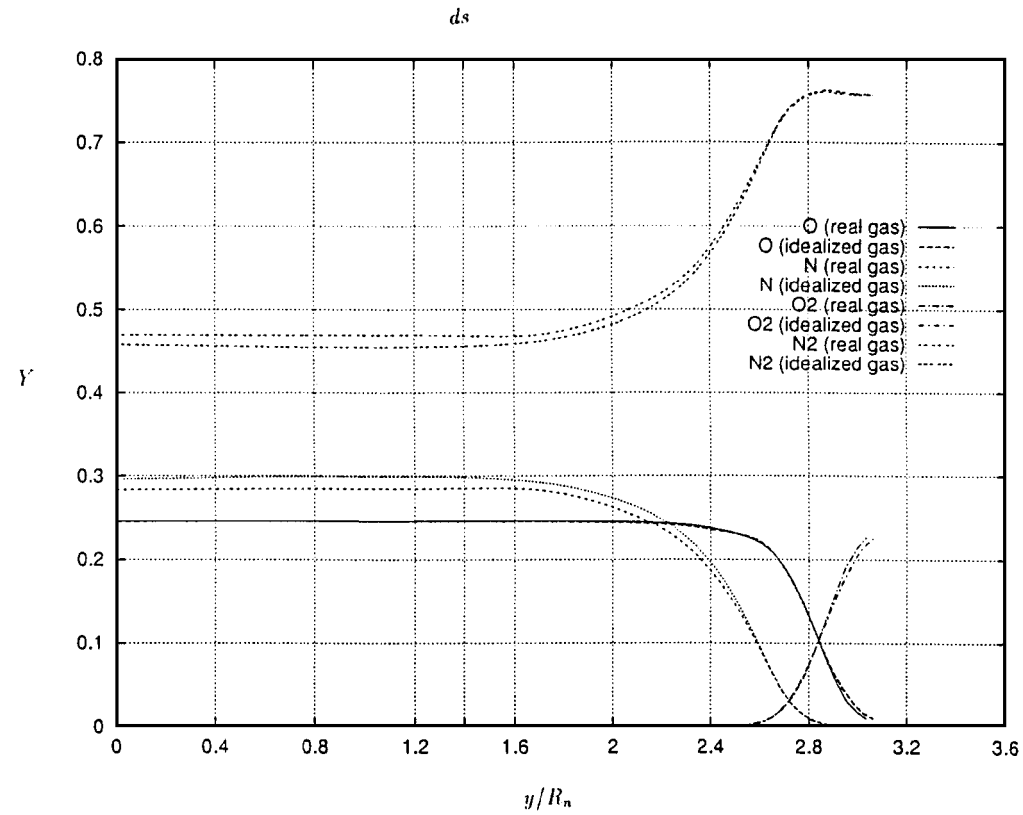

a) Heavy neutral-species mass fractions

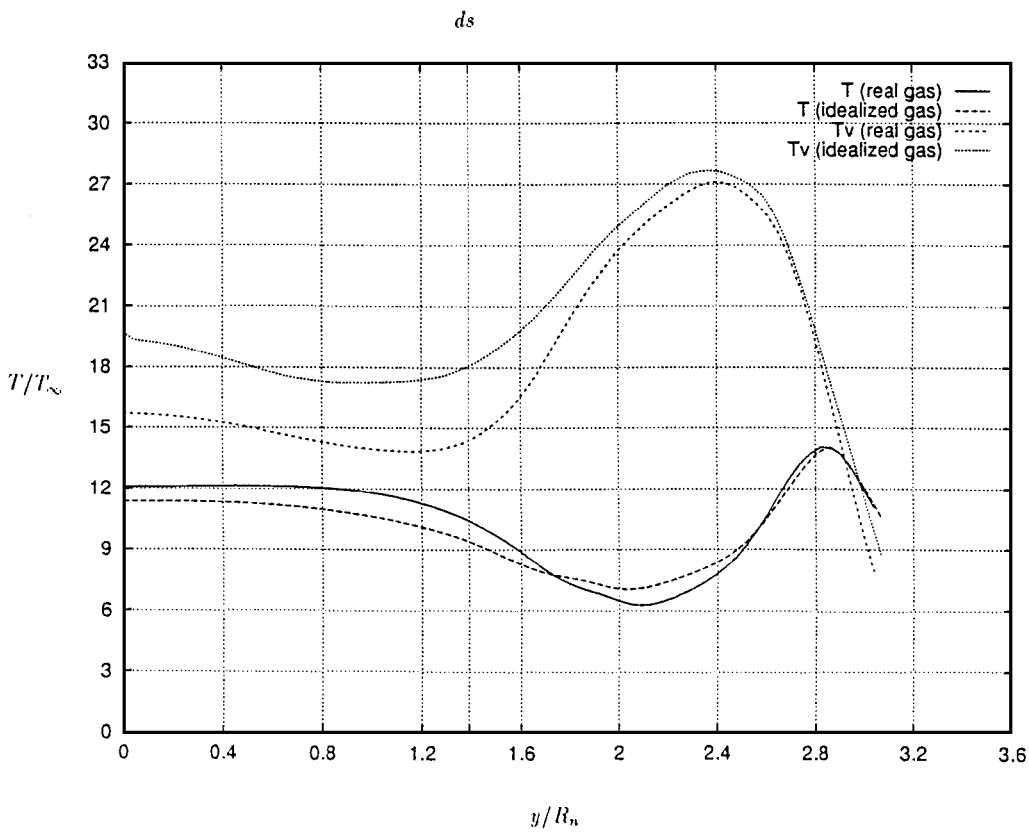

b) Translational and vibrational temperatures

Fig. 12 Radial distributions of idealized-gas simulation results in recirculation core for test case A.

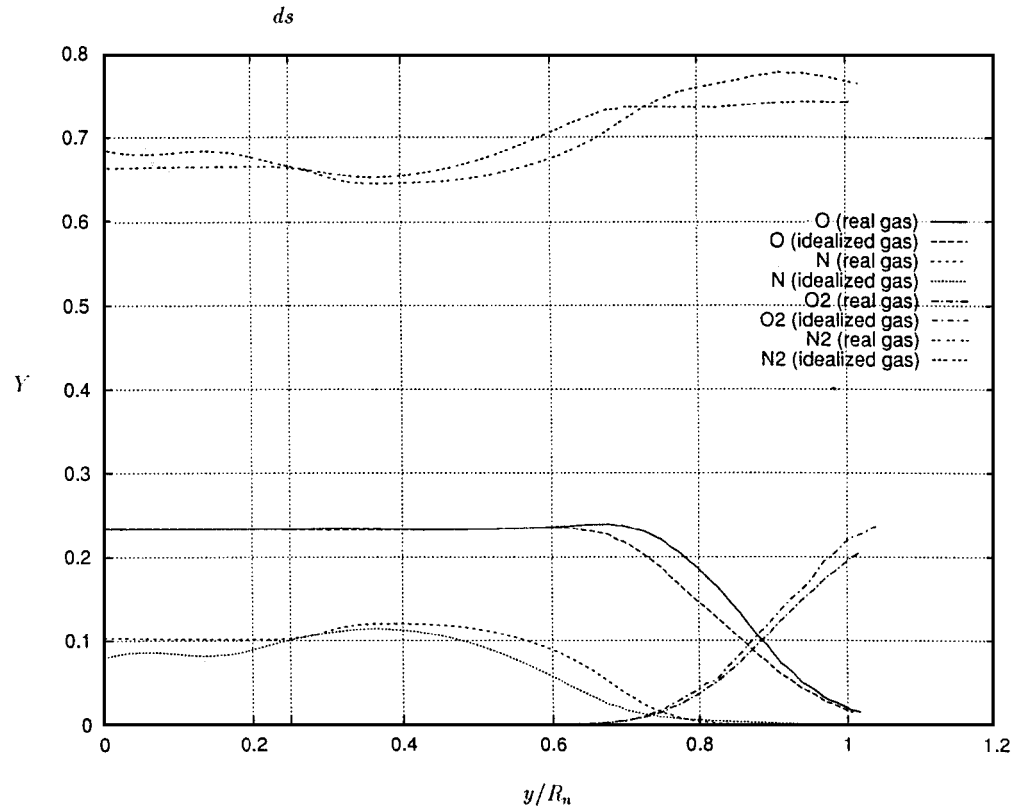

a) Heavy neutral-species mass fractions

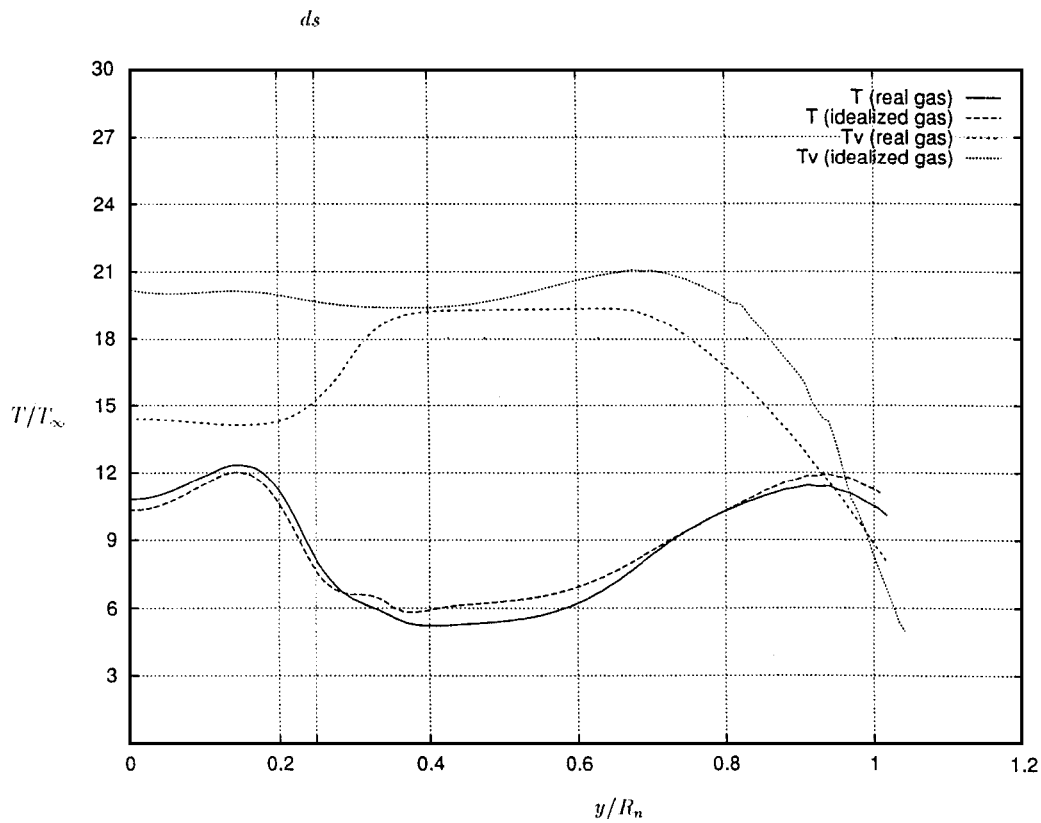

b) Translational and vibrational temperatures

Fig. 13 Radial distributions of idealized-gas simulation results in recirculation core for test case E.

Table 2 Comparison between real-gas (*R*) and idealized-gas (*I*) models

Test	Model	Re_{ds}	δ_s	Re_{sh}	M_{sh}	ℓ_w	δ_w	Δs	$\Delta\ell$	M_{ds}	M_{ax}	St_{peak}
A	R	1.5444×10^2	3.62*e*–2	7.5816×10^3	5.37	5.715	1.17	0.0780	0.385	0.941	0.822	0.257*e*–2
A	$I(X_{RI}=7.863)$	1.5799×10^2	3.45*e*–2	7.0502×10^3	5.05	5.699	1.06	0.0886	0.381	0.966	0.938	0.242*e*–2
A	$I(\Delta X_{RI}=-\Delta\ell)$	1.6518×10^2	3.64*e*–2	6.1621×10^3	4.71	5.707	1.08	0.0867	0.411	0.972	0.939	0.241*e*–2
A	$I(\Delta X_{RI}=+\Delta\ell)$	1.6639×10^2	3.39*e*–2	6.6798×10^3	4.93	5.665	1.06	0.0879	0.325	0.996	0.940	0.243*e*–2
A	$I(X_{RI}=4.273)$	1.6295×10^2	3.33*e*–2	7.2935×10^3	5.72	4.943	1.03	0.0924	0.381	0.968	0.925	0.241*e*–2
A	$\gamma=1.4$	1.5582×10^2	3.35*e*–2	6.4672×10^3	4.91	5.019	1.04	0.100	0.292	1.04	0.942	0.195*e*–2
A	$\gamma=1.465$	1.4432×10^2	3.39*e*–2	7.0555×10^3	5.07	4.996	1.07	0.1011	0.335	0.991	0.899	0.210*e*–2
E	R	3.8423×10^3	——	——	——	1.088	0.1205	——	——	1.595	1.471	0.113*e*–2
E	$I(X_{RI}=0.1563)$	3.8333×10^3	——	——	——	1.007	0.1274	——	——	1.710	1.490	0.131*e*–2
E	$I(X_{RI}=0.1016)$	4.2510×10^3	——	——	——	0.8756	0.1172	——	——	1.613	1.296	0.871*e*–3
E	$\gamma=1.4$	3.5905×10^3	——	——	——	0.965	0.1102	——	——	1.680	1.609	0.687*e*–3
E	$\gamma=1.476$	3.3255×10^3	——	——	——	1.049	0.1124	——	——	1.617	1.465	0.692*e*–3

because of space limitations), $Re_{ds}\simeq\mathcal{O}(10^3)$ and a constant vorticity core is detected with a convection-like behavior, thus supporting the conclusions reached previously[2] even for nonequilibrium flows.

Idealized-Gas Simulations

The idealized-gas model has been applied to simulate both the flow around the RAM-C and the ARC geometries at conditions corresponding to test cases A and E of Table 1. Results are reported in Table 2, which clearly shows that the properties of the wake are remarkably well predicted when the idealized-gas model is used. The isopressure contour lines of the idealized and the full nonequilibrium solutions are reported in Figs. 10 and 11, which show that the flow details are very well predicted.

The sensitivity of the solution to X_{RI}, i.e., the location at which the idealized-gas model is initialized, also has been assessed for both test cases. For test case A, we first considered a reference test case with $X_{RI}=7.863$, i.e., before the region of upstream influence, then two additional cases by varying the interface location by an amount of $\Delta X_{RI}=\pm\Delta\ell$, and finally a test with $X_{RI}=1.273$, i.e., at about half length of the cone. The results, as shown in Table 2, seem to indicate that the characteristic parameters of the flow are rather insensitive to X_{RI} (recall that, for this geometry, nonequilibrium effects are confined to the nose region), even when the interface location is inside the region of upstream influence ($\Delta X_{RI}=\Delta\ell$), except for the extent of the upstream influence zone. With regard to test case E, we performed two calculations, one with $X_{RI}=0.1563$, i.e., immediately past the shoulder, and one with $X_{RI}=0.1016$, i.e., before the shoulder. Results indicate that the former simulation captures very well the main flow features, whereas the latter shows several discrepancies, and thus a significant sensitivity to X_{RI}. This fact can be explained by observing that, for the ARC geometry, nonequilibrium effects are important in the entire forebody region, and an idealized-gas model, strictly valid for nearly frozen-flow conditions, is expected to fail.

To show the usefulness of the idealized-gas model, we also present a comparison with calculations performed with constant γ initialized at $X_{RI}=7.863$ for test case A and at $X_{RI}=0.1563$ for test case E. Two values of γ have been considered for both test cases: one with the classic value of $\gamma=1.4$ and one with a value obtained as the average of the ratio of h over e at X_{RI}. The constant γ results show an underestimation of both the upstream influence and the extent of the recirculation and an overestimation of the separation location. Another important parameter of the near wake is the peak heating along the base, which is defined in terms of the Stanton number $\{St=q/[\rho_\infty v_\infty(h_{0,\infty}-h_w)]\}$. Table 2 shows that the peak heating on the base can be predicted with the idealized model with an accuracy of $\mathcal{O}(10$–$15\%)$, whereas constant γ simulations are far less accurate.

The species concentrations and the vibrational temperature are well reproduced (with a 10-fold saving in computational time); their distributions in the recirculation region are reported in Figs. 12 and 13. The predictions of the main species (O, N, and N_2) show a very good agreement both for the RAM-C and ARC geometries; however, for the trace species (NO, NO^+, and e−, not reported), the agreement is only qualitative (but still satisfactory). Likewise, the vibrational temperature is also well recovered, except along the axis of the wake, where differences of the order of 30% are found.

Conclusions

We have evaluated the influence of real-gas effects on the structure of near wakes, and we have developed an idealized-gas model that is capable of accounting for real-gas effects. The study is confined to flows around simple sphere–cone geometries and ARCs and confirms that near-wake flows can be assumed to be both thermally and chemically frozen. Nevertheless, the forebody nonequilibrium affects the upstream influence, the separation location along the base, the extent of the recirculation, the thickness of the wake neck, etc. As a consequence, real-gas effects cannot be entirely neglected.

The study shows that the quantities that characterize the near-wake behavior satisfy scaling laws that depend on the dividing streamline Reynolds number and forebody boundary-layer properties, on the specific-heat ratio, and on the local mixture composition. In addition, we show that the main effects due to nonequilibrium can be accounted for by means of an idealized-gas model that solves for the compressible Navier–Stokes equations and a transport equation for the specific-heat ratio, supplemented with algebraic relations to determine the species mass fractions and vibrational temperature as a function of γ.

References

[1]Gnoffo, P. A., Price, J. M., and Braun, R. D., "On the Computation of Near Wake, Aerobrake Flowfields," AIAA Paper 91-1371, June 1991.

[2]Grasso, F., and Pettinelli, C., "Analysis of Laminar Near-Wake Hypersonic Flows," *Journal of Spacecraft and Rockets*, Vol. 32, No. 6, 1996, pp. 970–980.

[3]Palmer, G., "The Development of an Explicit Thermochemical Nonequilibrium Algorithm and Its Applications to Compute Three Dimensional AFE Flowfields," AIAA Paper 89-1701, June 1989.

[4]Venkatapathy, E., Palmer, G., and Prabhu, D. K., "AFE Base Flow Computations," AIAA Paper 91-1372, June 1991.

[5]Dogra, V. K., Moss, J. N., and Price, J. M., "Near-Wake Structure for a Generic Configuration of Aeroassisted Space Transfer Vehicle," *Journal of Spacecraft and Rockets*, Vol. 31, No. 6, 1994, pp. 953–959.

[6]Kim, M. S., Loellbach, J. M., and Lee, K. D., "Effects of Gas Models on Hypersonic Base Flow Calculations," *Journal of Spacecraft and Rockets*, Vol. 31, No. 2, 1994, pp. 223–230.

[7]Mitcheltree, R. A., and Gnoffo, P., "Wake Flow About the Mars Pathfinder Entry Vehicle," *Journal of Spacecraft and Rockets*, Vol. 32, No. 5, 1995, pp. 771–776.

[8]Vincenti, W. G., and Krueger, C. H., Jr., *Introduction to Physical Gas Dynamics*, Wiley, New York, 1965, pp. 120–139.

[9]Grasso, F., and Bellucci, V., "Thermal and Chemical Non Equilibrium Hypersonic Flow Computations," AGARD-70 FDP, Paper 43, May 1992.

[10]Park, C., *Nonequilibrium Hypersonic Aerothermodynamics*, Wiley, New York, 1990, pp. 119–143.

[11]Gupta, R. N., Yos, J. M., Thompson, R. A., and Lee, K. P., "A Review of Reaction Rates and Thermodynamic and Transport Properties for an 11-Species Air Model for Chemical and Thermal Nonequilibrium Calculations to 30,000 K," NASA RP 1232, 1990.

[12]Grasso, F., and Capano, G., "Modeling of Ionizing Hypersonic Flows in Non-Equilibrium," *Journal of Spacecraft and Rockets*, Vol. 32, No. 2, 1995, pp. 217–224.

[13]Lee, J. H., "Basic Governing Equations for the Flight Regimes of Aeroassisted Orbital Transfer Vehicles," *Thermal Design of Aeroassisted*

Orbital Transfer Vehicles, edited by H. F. Nelson, Vol. 96, Progress in Astronautics and Aeronautics, AIAA, New York, 1985, pp. 3–53.

[14]Gnoffo, P. A., and Gupta, R. N., "Conservation Equations and Physical Models for Hypersonic Air Flows in Thermal and Chemical Non-Equilibrium," NASA TP 2867, 1989.

[15]Millikan, R. C., and White, D. R., "Systematics of Vibrational Relaxation," *Journal of Chemical Physics*, Vol. 39, No. 12, 1963, pp. 3209–3213.

[16]Deiwert, G. S., and Candler, G. V., "Three-Dimensional Supersonic and Hypersonic Flows Including Separation," AGARD Rept. 764, May 1989.

[17]Appleton, J. P., and Bray, K. N. C., "The Conservation Equations for a Nonequilibrium Plasma," *Journal of Fluid Mechanics*, Vol. 20, No. 4, 1964, pp. 659–672.

[18]Grasso, F., and Marini, M., "Solutions of Hypersonic Viscous Flows with Total Variation Diminishing Multigrid Techniques," *Computers and Fluids Journal*, Vol. 23, No. 5, 1995, pp. 571–592.

[19]Larrouturou, B., "How to Preserve the Mass Fractions Positivity When Computing Compressible Multi-Component Flows," *Journal of Computational Physics*, Vol. 95, No. 1, 1991, pp. 59–84.

[20]Grantham, W. L., "Flight Results of a 25,000 fps Re-Entry Experiment," NASA TN D-6062, 1970.

[21]Hama, F. R., "Experimental Studies on the Lip Shock," *AIAA Journal*, Vol. 6, No. 2, 1968, pp. 212–219.

K. Kailasanath
Associate Editor